THE PROTEIN SOCIETY

The dynamics of interleukin-8 and its interaction with human CXC receptor I peptide

Agnieszka A. Kendrick,[1] Michael J. Holliday,[1] Nancy G. Isern,[2] Fengli Zhang,[3] Carlo Camilloni,[4] Chi Huynh,[1] Michele Vendruscolo,[4] Geoffrey Armstrong,[5] and Elan Z. Eisenmesser[1]*

[1]Department of Biochemistry and Molecular Genetics, School of Medicine, University of Colorado Denver, Aurora, Colorado 80224

[2]WR Wiley Environmental Molecular Sciences Laboratory, High Filed NMR Facility, Richland, Washington 99532

[3]National High Magnetics Field Laboratory, Tallahassee, Florida 32310

[4]Department of Chemistry, University of Cambridge, Cambridge CB2 1EW, United Kingdom

[5]Department of Chemistry and Biochemistry, University of Colorado at Boulder, Boulder, Colorado 80309

Received 16 October 2013; Revised 13 January 2014; Accepted 16 January 2014
DOI: 10.1002/pro.2430
Published online 20 January 2014 proteinscience.org

Abstract: Interleukin-8 (CXCL8, IL-8) is a proinflammatory chemokine important for the regulation of inflammatory and immune responses via its interaction with G-protein coupled receptors, including CXC receptor 1 (CXCR1). CXCL8 exists as both a monomer and as a dimer at physiological concentrations, yet the molecular basis of CXCL8 interaction with its receptor as well as the importance of CXCL8 dimer formation remain poorly characterized. Although several biological studies have indicated that both the CXCL8 monomer and dimer are active, biophysical studies have reported conflicting results regarding the binding of CXCL8 to CXCR1. To clarify this problem, we expressed and purified a peptide (hCXCR1pep) corresponding to the N-terminal region of human CXCR1 (hCXCR1) and utilized nuclear magnetic resonance (NMR) spectroscopy to interrogate the binding of wild-type CXCL8 and a previously reported mutant (CXCL8M) that stabilizes the monomeric form. Our data reveal that the CXCL8 monomer engages hCXCR1pep with a slightly higher affinity than the CXCL8 dimer, but that the CXCL8 dimer does not dissociate upon binding hCXCR1pep. These investigations also showed that CXCL8 is dynamic on multiple timescales, which may help explain the versatility in this interleukin for engaging its target receptors.

Keywords: interleukin-8; dimer; human CXC receptor 1; NMR; dynamics

Introduction

Interleukin-8 (IL-8, CXCL8) is a member of the pro-inflammatory CXC cytokine family implicated in mediation of inflammatory responses, including angiogenesis, leukocyte degranulation and cell migration.[1,2] CXC chemokines are small proteins (8–12 kDa) that contain a conserved CXC residue motif (C-cysteine, X-any other residue) proximal to the N-terminal region of the protein.[3] Solution and solid-state structures of several human CXC chemokines have been solved, revealing a common tertiary

Abbreviations: CPMG, Carr-Purcell-Meiboom-Gill; CXCL8, interleukin-8; HMQC, heteronuclear-multi-quantum-coherence; HSQC, heteronuclear-single quantum coherence; NMR, nuclear magnetic resonance; R1, longitudinal relaxation rate; R2, transverse relaxation rate.

Additional Supporting Information may be found in the online version of this article.

Grant sponsor: Department of Energy's Office of Biological and Environmental Research. Grant sponsor: The Rocky Mountain 900 Facility; Grant number: NIHGM68928.

*Correspondence to: Elan Zohar Eisenmesser, Department of Biochemistry and Molecular Genetics, School of Medicine, University of Colorado Denver, Aurora, CO 80045. E-mail: Elan.Eisenmesser@UCDenver.edu

fold for all members of the family consisting of an unstructured N-terminal loop, antiparellel β-strands and a C-terminal α-helix.[4] CXC chemokines typically dimerize, and residues within the first β-strand and α-helix are important for the stabilization of the dimeric form.[3] In CXCL8, dimerization occurs via an interaction between side chains in its first β-strand and is further stabilized by its C-terminal α-helix and two disulphide bridges (Cys7-Cy34 and Cy9-Cys50). Several different mutations or truncations that disrupt the structural order in these regions can lead to formation of dimerization-incapable CXCL8 mutants, which include deletion of C-terminal residues involved in α-helix formation and mutation of the residues within one of the β-strands.[5–8]

Although several studies have characterized the importance of dimerization on the activity of CXCL8 *in vitro* and *in vivo*, the molecular and functional consequences of such dimerization are not known in full detail. The dissociation constant (K_d) for CXCL8 dimerization has been reported to be 10 to 20 μM.[7,9] As CXCL8 is secreted at high concentrations from injured or cancerous tissues, its local concentration can vary significantly, leading to the existence of both the monomeric and dimeric forms at different locations and over time.[10,11] This differential distribution of the CXCL8 dimeric and monomeric forms may suggest an important role for each of them in the functional activity of this chemokine. For example, one may hypothesise that the formation of CXCL8 dimers at high concentrations may diminish the binding affinity of CXCL8 to its receptors, and thereby serve as a control mechanism to downregulate signaling.

The predominant naturally-occuring form of wild-type CXCL8 comprises 72 residues (1–72, herein termed as wild-type CXCL8) and is obtained after cleavage of the precursor form, leading to the removal of five N-terminal residues. Biological studies have shown that the precursor form of CXCL8 is less active, supporting the biological importance of studying the mature, wild-type CXCL8.[12] CXCL8 interacts with two G-protein coupled receptors, CXCR1 and CXCR2, resulting in a diverse array of signaling events linked to the regulation of tumor microenvironment in breast, pancreatic, and prostate cancers.[1,13] CXCR1 is targeted by CXCL8 and granulocyte chemotactic protein-2 (GCP-2) only, while CXCR2 is targeted by CXCL8 and several other ligands. These two receptors are highly homologous, with the only major differences being in the extracellular N-terminal region implicated in ligand binding, thus explaining their specificity for their particular ligands.[14] Several studies have characterised the CXCL8 interaction with CXCR1 as a two-site process. Site I comprises the initial interaction between the CXCL8 N-loop residues and the CXCR1 receptor N-terminal residues, while site II involves the CXCL8 N-terminal (ELR motif) and the receptor distant extracellular region.[5–7,10,14–16] However, a recent biophysical study performed in lipid bilayers using human full-length CXCR1 and CXCL8 did not fully support such findings, suggesting that the binding process between CXCL8 and human CXCR1 appears to be mainly associated with the N-terminal region of the receptor.[17] Furthermore, using biophysical studies, Ravindran *et al.*[7] proposed that upon receptor engagement, wild-type CXCL8 dissociates to form a CXCL8 monomer/receptor complex. In contrast with these results, CXCL8 dimerization has been shown to be critical for neutrophil recruitment, one of the major CXCL8 roles in regulating inflammatory responses.[18] These discrepancies may arise from the fact that most biophysical studies to date have been conducted with a peptide corresponding to the residues within the N-terminal region of a rabbit CXCR1 homolog, as opposed to its human counterpart, while biological studies reflect the interaction with the human CXCR1 (hCXCR1) sequence.

For the present study, we expressed and purified both CXCL8 and a peptide corresponding to residues 9 to 29 of hCXCR1 (herein referred to as hCXCR1pep). Using these constructs, we characterized the interaction of hCXCL8 and the hCXCR1 N-terminal region by solution NMR titration and relaxation studies. We also generated a previously described[8] double-mutant to disrupt the dimerization interface in order to obtain a monomeric form of CXCL8 (herein referred to as CXCL8M), and thereby perform comparative biophysical studies with the CXCL8 dimeric and monomeric forms. Our data support the conclusion that the interaction of CXCL8 with the hCXCR1 peptide is specific, but, importantly, also reveal that wild-type CXCL8 persists in a dimeric form upon engagement of the receptor peptide without the prerequisite of dimer dissociation. Additionally, our backbone amide NMR relaxation data demonstrate evidence that CXCL8 exhibits an inherent mobility, suggesting that the dynamic nature of CXCL8 might contribute to its ability to target multiple receptors.

Results

CXCL8 monomers bind hCXCR1pep weakly but specifically, and with higher affinity than CXCL8 dimers

To test the binding of human CXCL8 to its human target receptor we expressed and purified a peptide corresponding to the N-terminal region of human CXCR1 [hCXCR1pep, Fig. 1(A)]. Previous studies attempting to characterize the interaction of CXCL8 with hCXCR1 used peptides spanning residues 1 to 40 of hCXCR1 N-terminal region or a shorter

construct.[9,19] Comparable binding characteristics were reported with either a truncated shorter peptide (residues 9–29) or a truncated peptidomimetic (residues 15–19 replaced by a chemical linker). Therefore, we chose the peptide corresponding to residues 9–29 of hCXCR1. We performed initial experiments using a CXCL8 construct generated with a 6xHis tag and a thrombin cleavage site that contained an N-terminal overhang after thrombin cleavage [Fig. 1(B)]. Additionally, to test the contribution of dimerization to the binding process, we generated a dimerization-incapable mutant form of CXCL8 by performing site-directed mutagenesis within the dimerization domain as previously described [Fig. 1(B,C)].[8] While both wild-type and monomeric constructs were initially generated with an N-terminal overhang resulting from thrombin cleavage (herein called $CXCL8^{Synthetic}$ and $CXCL8M^{Synthetic}$, respectively), these constructs were also generated using a Factor Xa cleavage site that allowed us to also test the biologically mature forms that do not comprise any overhang (herein called CXCL8 and CXCL8M). Each construct was well folded and behaved as a dimer and a monomer, respectively, based on NMR data (Supporting Information Fig. S1) and size-exclusion chromatography (data not shown). Comparative studies between the synthetic and the biological form have allowed us to account for the importance of the CXCL8 N-terminus in the binding interaction [Fig. 2]. $^{1}H/^{15}N$ heteronuclear single-quantum coherence (HSQC) solution NMR experiments were used to assess the binding interface and affinity through chemical shift perturbations. Unlabeled hCXCR1pep was titrated into ^{15}N-labeled CXCL8 constructs, and binding induced chemical shift perturbations were monitored upon peptide engagement.

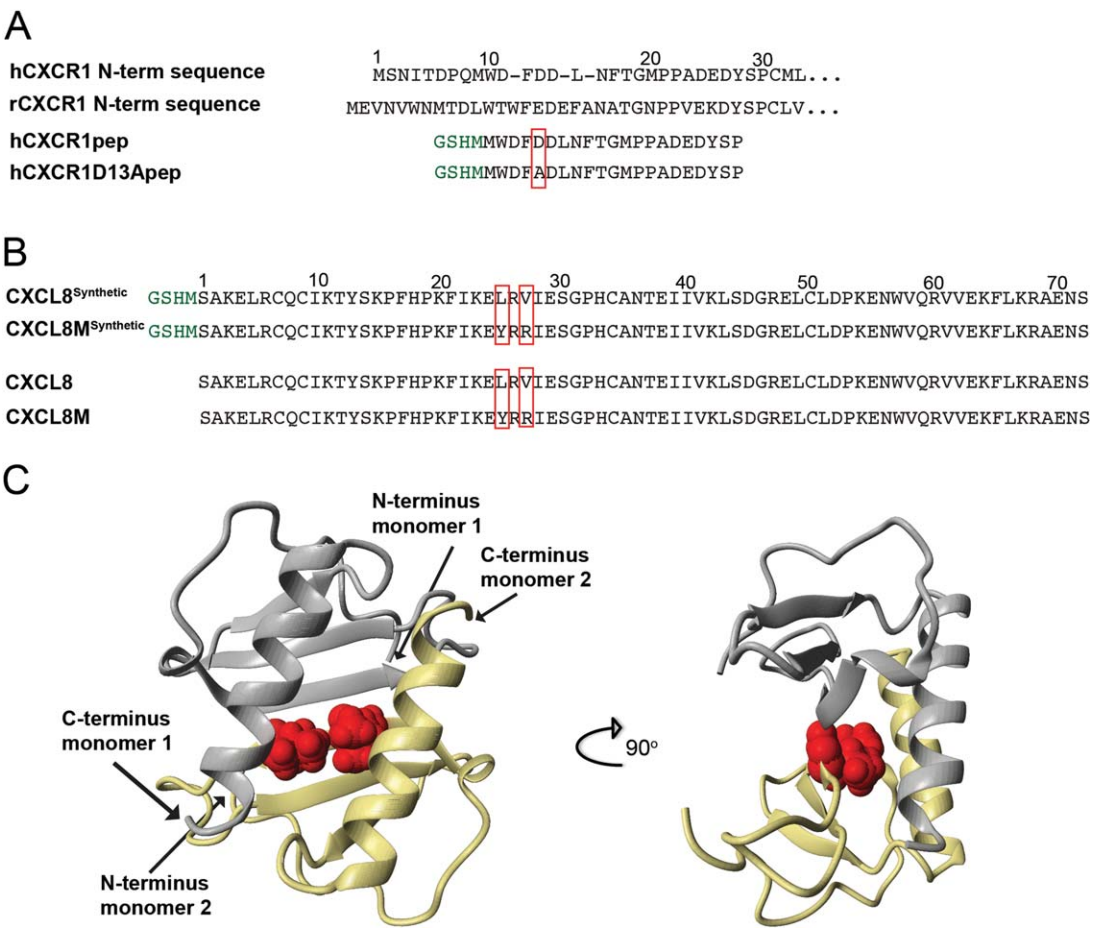

Figure 1. Sequence of the CXCR1 N-terminal region, and sequence and structure of interleukin-8 (CXCL8). (A) Alignment of the amino acid sequence of the human CXCR1 (hCXCR1) N-terminal region with that of the rabbit CXCR1 (rCXCR1) Nterminal region. The peptide used in the study (hCXCR1pep) and the binding mutant (hCXCR1D13Apep) are also shown, with the post-purification overhang highlighted in green. (B) Amino acid sequences of human CXCL8 constructs utilized in the study. The postpurification overhang residues are highlighted in green and constructs containing such overhangs are described as synthetic. The double mutation that blocks CXCL8 dimerization and is thus a CXCL8 monomer (L25Y and V27R) is highlighted in red box. (C) Ribbon diagram of the CXCL8 dimer crystal structure. N- and C-termini of each monomer are labeled and the residues (L25 and V27) mutated to form monomer are mapped onto one of the monomers. PDB code 3IL8, Human CXCL8 GenBank accession code 3576, hCXCR1 GenBank accession code L19591, rCXCR1 GenBank accession code M58021.

Previously reported binding affinities vary significantly and such discrepancies may have arisen from the various conditions and/or specific constructs used as shown below.[7,9,12,19,20] Therefore, we sought to specifically test the sensitivity of CXCL8/hCXCR1pep binding to such variations in a more comprehensive manner by performing our experiments using some of the previously reported buffers and CXCL8 constructs. Specifically, initial titrations were completed in the presence of phosphate buffer at pH 6.5 for synthetic CXCL8 constructs [Fig. 2(A)]. Although both synthetic CXCL8 constructs engaged hCXCR1pep, the monomer exhibited slightly tighter binding as determined by chemical shift perturbations and the associated binding isotherms with dissociation constants of 544 ± 25 μM for $CXCL8^{Synthetic}$ and 440 ± 30 μM for $CXCL8M^{Synthetic}$ [Fig. 2(A)]. Since these interactions were relatively weak, we next sought to determine whether they were specific. The contribution of the single Asp13 residue within the hCXCR1pep to binding was surmised based on reverse titrations where we added unlabeled $CXCL8^{Synthetic}$ into ^{15}N-labeled hCXCR1pep that we had previously assigned (Supporting Information Fig. S2A). The largest chemical shift changes in carbon Cα and Cβ were observed for Asp13 of hCXCR1pep upon binding CXCL8 (Supporting Information Fig. S2B), providing initial evidence as to the electrostatic nature of this interaction. Consistent with this conclusion, an Asp13→Ala mutant hCXCR1pep showed marked reduction in binding affinity to $CXCL8^{Synthetic}$ with a dissociation constant of 1.3 ± 0.05 mM (Supporting Information Fig. S2C). Interestingly, while there have been mutagenesis studies of the hCXCR1 N-terminal region, Asp13 has not been previously characterised as important for binding[21] and thus, in addition to revealing specificity, our studies have identified a primary contribution to the CXCL8/CXCR1 interaction. Similar affinities to the $CXCL8^{Synthetic}$ were obtained upon using the wild-type CXCL8 constructs [Fig. 2(B)], with 550 ± 26 μM and 460 ± 27 μM for CXCL8 and CXCL8M, respectively. Consistent with the conclusion that electrostatics play an important role in the CXCL8/hCXCR1pep interaction, a significant increase in binding affinities was detected when titrations were performed in the presence of HEPES buffer instead of phosphate buffer [Fig. 2(C)]. Unfortunately, we were not able to confidently determine the binding affinity for wild-type constructs in the HEPES buffer due to slight sample precipitation that was especially evident for CXCL8M. However, a comparison of the chemical shift perturbations at the first few titration points, prior to precipitation, reveals significantly larger shifts in HEPES buffer, relative to the ones collected in phosphate buffer, consistent with a higher binding affinity. This observation is consistent with other studies in HEPES buffer that reported a dissociation constant of 10 μM using Isothermal Titration Calorimetry.[15] Although both HEPES and phosphate buffers are routinely utilized to mimic physiological conditions, the actual biological environment is more complicated because of the presence of a variety of other molecular species. Hence, the binding affinities measured in those buffers are likely to be influenced by other factors (e.g. other ions or proteins). Based on our NMR titrations data we can conclude that the interaction between CXCL8 and CXCR1pep involves a number of charged residues, which are described below, suggesting that the nature of this interaction is primarily electrostatically driven. This electrostatic interaction would likely be masked by high ionic strength buffers (i.e. phosphate buffer), consistent with our aforementioned results. In summary, our studies indicate that: (i) the CXCL8 monomer binds hCXCR1pep with a slightly higher affinity than the CXCL8 dimer, (ii) modifications to the N-terminal region of CXCL8 bear little consequence to binding, and (iii) the CXCL8/hCXCR1pep interaction is primarily electrostatic.

The peak widths observed in the $^{1}H/^{15}N$ NMR spectra during titrations suggest that the exchange process is in a fast NMR time regime, which is consistent with the relatively weak binding constants determined above. Based on the previously published crystal structure of CXCL8,[22] we can deduce that residues exhibiting the largest chemical shift perturbations are located in the N-terminal loop (Thr12, Phe17, His18, Phe21), the turn preceding β3-strand (Ser44, Asp45), β3-strand (Glu48, Leu49, Cys50), and the C-terminal α-helix (Val61 and Val62). A mapping of these residues onto the crystal structure reveals that they are highly localized [Fig. 2(D) and Supporting Information Fig. S3A]. With the exception of residues Asp45 and Val62, the chemical shift interface determined from chemical shifts is in agreement with previously published studies describing similar regions within CXCL8 for the interaction with the longer or modified hCXCR1 peptide.[9,19] The binding interface changed only marginally for the monomeric form of CXCL8 (Supporting Information Fig. S3B), with the involvement of additional residues exhibiting perturbations within the first β-strand (Tyr25 and Arg26) and the α-helical region (Lys67 and Arg68). For all CXCL8 constructs we did not observe any significant chemical shift perturbations for the N-terminal region (ELR motif), suggesting that these residues are not critical for the N-terminal hCXCR1 peptide interaction. This lack of the CXCL8 ELR motif involvement in binding is consistent both with our results that detected similar affinities for the synthetic and wild-type N-termini of CXCL8 above, as well as with several previous studies.[17,23]

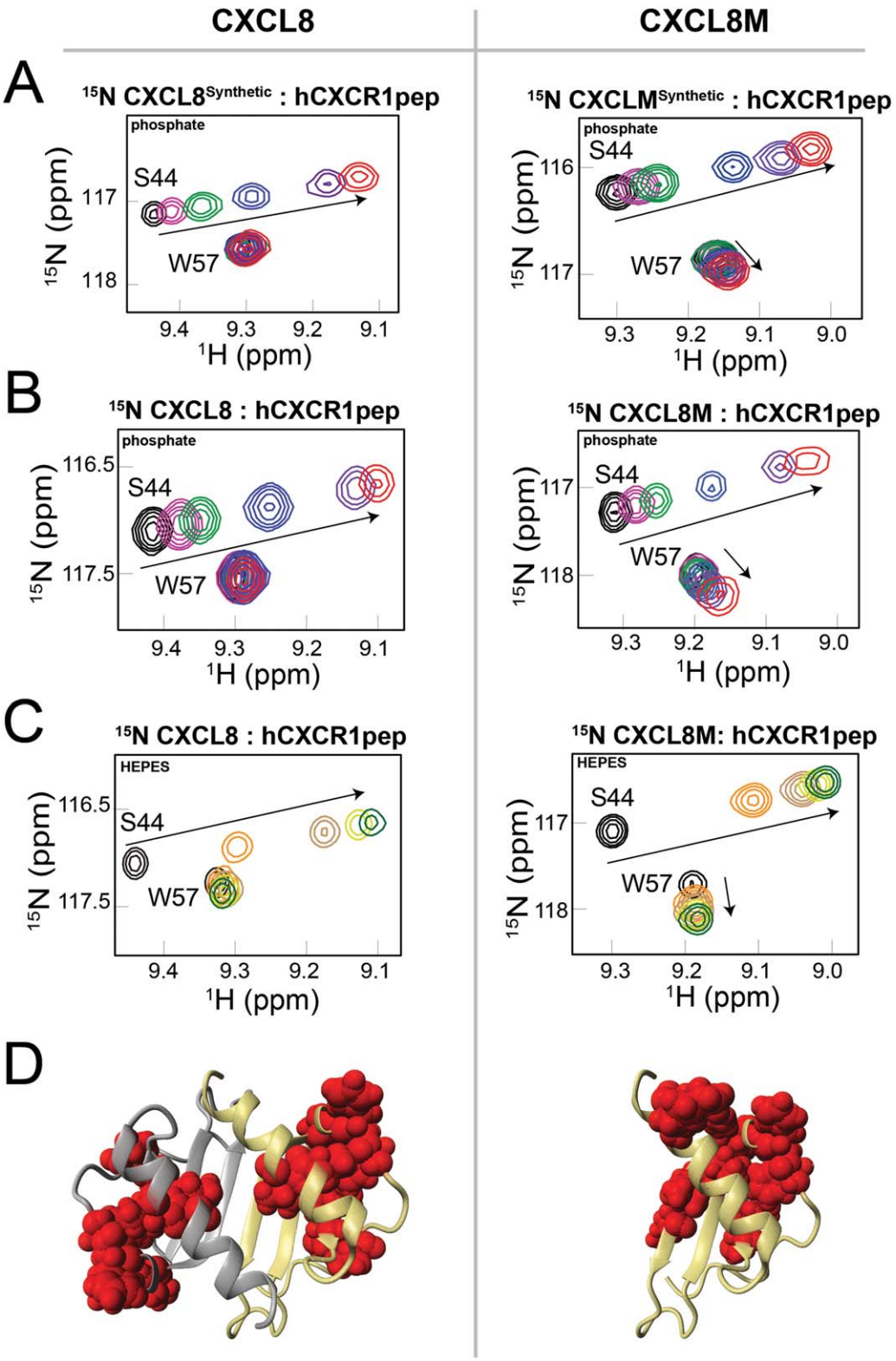

Figure 2. CXCL8 engages human CXCR1 peptide weakly with increased affinity in the monomeric CXCL8 form. (A–C) Expanded regions of 1H/^{15}N HSQC NMR titration experiments for the uniformly ^{15}N labeled CXCL8 (left panels) and the monomeric CXCL8 mutant (right panels). Increased concentrations of unlabeled hCXCR1pep were titrated into ^{15}N labeled protein (black—free protein). (A) CXCL8Synthetic or CXCL8MSynthetic in 50 m*M* phosphate, 150 m*M* NaCl, pH 6.5; (B) CXCL8 or CXCL8M in 50 m*M* phosphate, 150 m*M* NaCl, pH 6.5; (C) CXCL8 or CXCL8M in 50 m*M* HEPES, 50 m*M* NaCl, pH 7.0. The molar ratios of the unlabeled hCXCR1pep to ^{15}N labeled protein were 0.2 (pink), 0.4 (green), 1.5 (blue), 4 (purple), 8 (red) in (A) and (B) and 0.25 (yellow), 0.5 (brown), 1 (light green), 2 (dark green) in (C). (D) Residues exhibiting normalized chemical change of 0.6 ppm or above (defined by $\sqrt{(5\Delta v_{1H})^2+(\Delta v_{15N})^2}$) upon hCXCR1pep peptide engagement are painted red on the CXCL8 dimer and monomer structures. PDB code 3IL8). All data were collected at 25°C at 900 MHz.

CXCL8 dimers do not dissociate upon hCXCR1pep engagement

CXCL8 dimer dissociation has been proposed to be a prerequisite for binding peptides derived from CXCR1.[11,16] The nature of the CXCL8 interaction with the hCXCR1 N-terminal region has been extensively characterized for the rabbit homolog,[5,16] but there are limited data available describing the interaction of human CXCL8 with its associated hCXCR1. Thus, to establish whether CXCL8 dimers dissociate upon binding to hCXCR1pep as previously proposed, we determined the correlation times (τ_c) of CXCL8 in its free and bound states, as this parameter is sensitive to molecular weight.[24] We collected R1 (longitudinal) and R2 (transverse) relaxation rates for backbone amides at 600 MHz, for both wild-type dimeric and mutated monomeric constructs in both free and hCXCR1pep bound states. Based on the dissociation constants described above, complete saturation was not possible in phosphate buffer but only in HEPES buffer. Thus, data are presented here in HEPES buffer (Fig. 3). However, comparable results were found in phosphate buffer as well [see Fig. 6(B) for the free state]. Under the sample conditions reported here, the average R1 relaxation rates for the free wild-type CXCL8 and CXCL8M constructs were approximately 1.4 s^{-1} and 2 s^{-1}, respectively [Fig. 3(A)], while in the bound states these averages change to 1 s^{-1} and 1.6 s^{-1}, respectively [Fig. 3(B)]. The average R2 relaxation rates were approximately 12 s^{-1}, and 8 s^{-1} for the free wild-type CXCL8 and CXCL8M constructs, respectively [Fig. 3(A)], while the bound states averages increased to 21 s^{-1} and 13 s^{-1}, respectively [Fig. 3(B)]. Based on the measured R2/R1 ratios, we calculated correlation times for the free and bound proteins using the equations described by Larsson *et al.*[24]

For free CXCL8 and CXCL8M, the calculated correlation times were 8.7 and 5.7 ns, respectively, and 14.9 and 8.9 ns for the bound counterparts, respectively. In folded proteins the effective correlation time relates well to the molecular weight of the protein up to 25 to 30 kDa.[25,26] The evaluation of correlation times allows for relatively accurate estimation of protein molecular weights.[24,27] Therefore, this method can readily be used to monitor protein dimerization and protein interactions in general, based on changes that alter molecular weight.[28,29] Using this established dependence of correlation time to molecular weight, we compared our experimental correlation times to a standard curve obtained from published correlation rates for known proteins [Fig. 3(C), black dots], which were acquired at the same temperature.[25,26] From these measurements, we estimated the molecular weight of free CXCL8 and CXCL8M to be 14.7 kDa and 9.4 kDa, respectively [Fig. 3(C), blue dots]. These values estimated from our experimental data correspond well to the molecular weights, calculated from the structure of the wild-type CXCL8 dimer (17 kDa) and CXCL8M monomeric form (8.6 kDa). We then extended our estimations to the relaxation data measured in the bound species providing molecular weights of 25.1 kDa and 15.2 kDa for the CXCL8 and CXCL8M complexes with hCXCR1pep, respectively [Fig. 3(C), green dots]. Considering that the wild-type CXCL8 dimer and hCXCR1pep are 17 kDa and 2.9 kDa, respectively, the molecular weight of CXCL8 dimer bound to two molecules of hCXCR1pep is 22.8 kDa (i.e., 17 kDa + 2 × (2.9 kDa)). This value agrees very well with the molecular weight estimated from our experimental data (25.1 kDa), which indicates that the dimer does not dissociate upon binding to the hCXCR1pep. Experimentally estimated molecular weight values for both CXCL8 and CXCL8M complexes were slightly higher than their actual molecular weights, which was likely due to the extended hCXCR1pep bound unstructured regions. However, the experimentally estimated molecular weight of wild-type CXCL8 dimer complex lies well within the bounds of a molecular weight of an intact dimer complex, and is much larger than that of the CXCL8 monomer complex [Fig. 3(C), green dots]. Similar values were obtained for the CXCL8 and CXCL8M constructs in phosphate buffer (Supporting Information Table S2). Collectively, these data indicate that CXCL8 does not dissociate upon receptor peptide engagement and, furthermore, the CXCL8 dimer stays intact with two molecules of hCXCR1pep bound per CXCL8 dimer. These findings are consistent with previous studies performed with another hCXCR1 peptide, but not with some of the conclusions utilizing a rabbit CXCR1 peptide that indicated dimer dissociation upon rabbit peptide binding.[7,15,23]

CXCL8 dynamics

Protein flexibility has been shown to play a critical role in enzyme-substrate and protein-ligand interactions, with binding sites and active sites often exhibiting inherent flexibility over multiple time regimes.[30–32] In order to determine whether a ligand such as CXCL8 may also be inherently dynamic within regions important for function, i.e., receptor engagement, we probed the dynamics on multiple time scales for CXCL8. R1 and R2 relaxation rates described above that allowed us to probe the molecular weight of CXCL8, both free and bound, can also be used to evaluate local mobility. These relaxation rates primarily report on the picosecond-nanosecond (ps-ns) time scale, with microsecond-millisecond (μs-ms) time scale motions (i.e., chemical exchange) contributing to large increases in the R2 relaxation rate that may also be probed by other methods (see below). For proteins that are in general outside of the "extreme narrowing limit" (i.e., τ_c>2.65 ns from

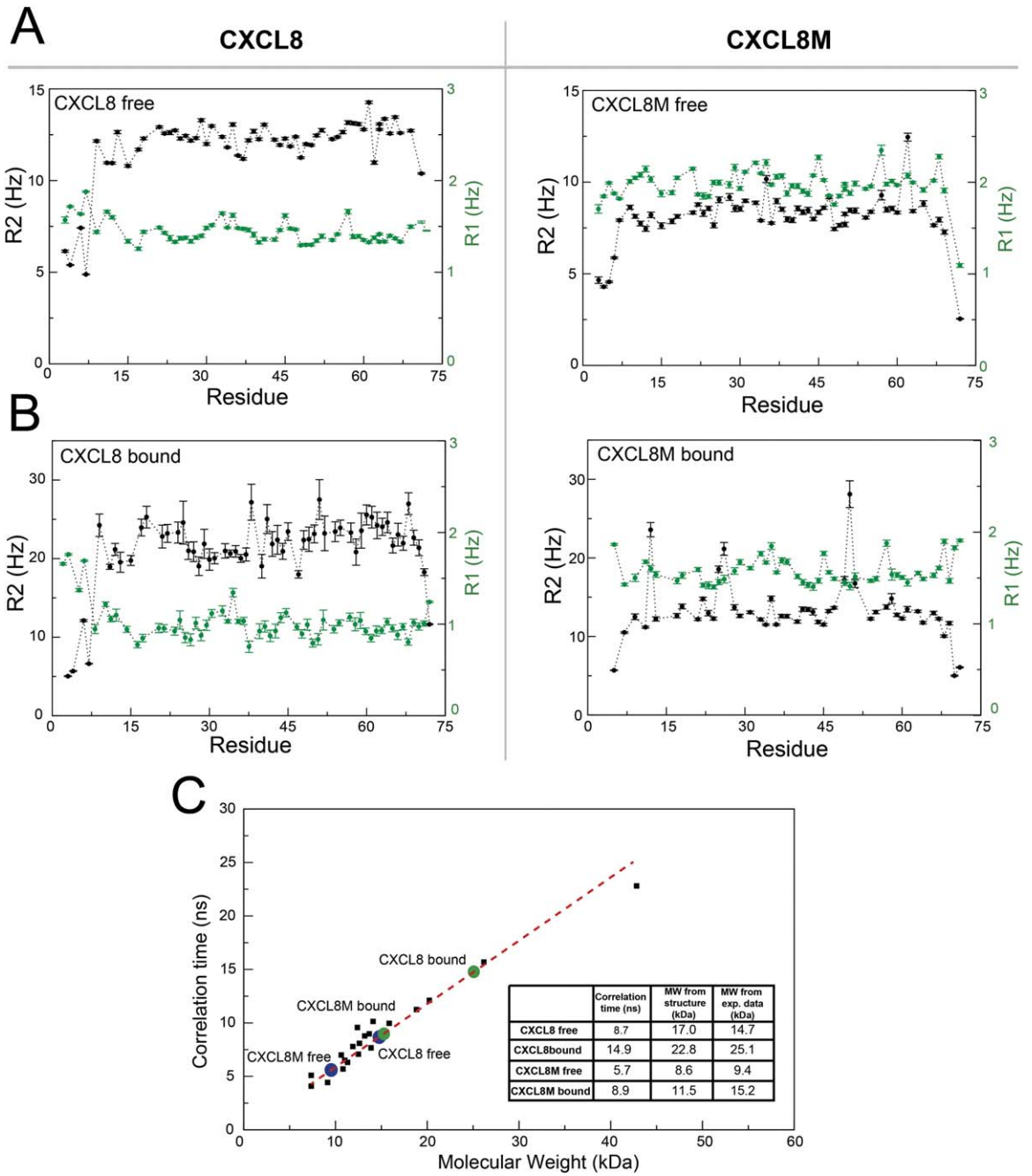

Figure 3. CXCL8 engagement of hCXCR1pep does not lead to dimer dissociation. NMR amide nitrogen R2 relaxation rates (black lines) and R1 relaxation rates (green lines) were collected for the free CXCL8 (A)—left panel, free CXCL8M (A)—right panel, bound CXCL8 (B)—left panel and bound CXCL8M (B) —right panel. (C) The extracted correlation times (τ_c) are plotted versus molecular weight (MW). The remaining values (black squares) are from previous studies that are also listed in Supporting Information Table 1. The MW values calculated from structures are listed in the table insert next to the MW values estimated from the experimental τ_c values. The MW, estimated from the experimental data was fitted into a first-order linear regression equation ($\tau_c = 0.59 \times$ MW). All data within this figure were collected in HEPES buffer at 25°C and 600 MHz.

$1/(2\pi\omega)$, with $\omega = 60.8$ MHz for ^{15}N on a 600 MHz spectrometer), relatively high R1 relaxation rates, together with low R2 relaxation rates, identify regions that exhibit a high degree of mobility, which indicates locally unstructured regions. This mobility is observed for several regions that include the N- and C-termini of the intact CXCL8 dimer [Figs. 3(A) and 6(B)]. Additional residues that exhibit small increase in R1 relaxation rates (within two standard deviations above the mean) are Ile11, Thr12, His33, Ala35, Asp45, and Trp57 [Figs. 3(A) and 4(C)]. His33 and Ala35 surround Cys34, which is located in a loop region and forms a disulfide bond with Cys7. The increase in mobility, as indicated by increase in

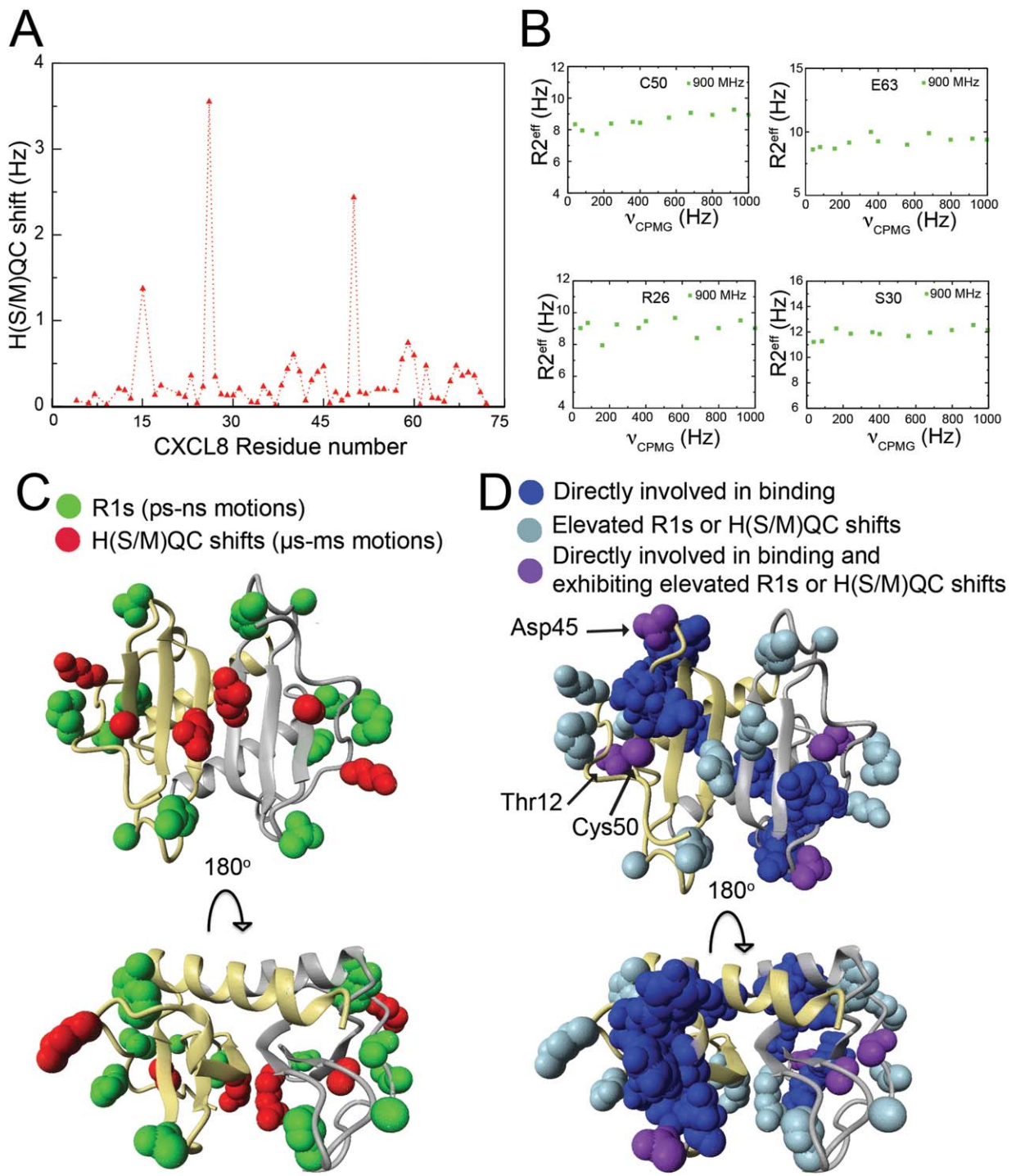

Figure 4. Multiple time scale dynamics of CXCL8. (A) Microsecond-millisecond (μs-ms) movements shown by the absolute value of H(S/M)QC exchange induced shifts. (B) Slow dynamics in wild type CXCL8 are primarily within the μs regime, as indicated by no R2-CPMG relaxation dispersion for representative residues (C50, E63, R26, and S30). (C) Structural summary of the detected motions within CXCL8, which include residues exhibiting elevated R1 relaxation rates that indicate local disorder on a fast timescale [green, see values in Fig. 3(A)] and H(S/M)QC exchange induced shifts that indicate exchange on the slow timescale (red). (D) Residues exhibiting elevated R1 relaxation rates and H(S/M)QC exchange induced shifts (gray) are mapped along residues directly involved in binding (blue). The three residues (purple and highlighted with arrows): Thr12, Asp45, and Cys50 exhibiting elevated R1 relaxation rates or H(S/M)QC exchange induced shifts and directly involved in binding. All residues mapped exhibited R1 rates and H(S/M)QC exchange induced shifts greater than one standard deviation above the average. PDB code 3IL8. All NMR experiments within this figure were collected in HEPES buffer at 25°C and 600 MHz.

R1 relaxation rates for these residues is likely due to their position in the flexible loop. Interestingly, Thr12 and Asp45 are both directly involved in binding hCXCR1pep [Fig. 4(D)]. Thus, one could propose that the increased flexibility of those amino acids may support the notion that residues may be flexible for function, which in this case is receptor binding. Finally, it should be noted that both the N- and C-termini of the monomeric CXCL8 mutant exhibit both low R1 and low R2 relaxation rates [Fig. 3(A), right panel] because these regions are so flexible that they actually lie within the extreme narrowing limit with calculated local correlation times lower than 2.65 ns.

In order to identify μs-ms motions, we also collected backbone exchange induced shifts using a combination of heteronuclear single-quantum coherence (HSQC) and homonuclear multiple-quantum coherence (HMQC), herein termed as H(S/M)QC shifts. This combination of two standard NMR experiments takes advantage of the fact that the residues undergoing chemical exchange on the μs-ms timescale give rise to small chemical shift changes between these two spectra.[33,34] The residues exhibiting elevated H(S/M)QC exchange induced shifts (greater than two standard deviations above the average) in the wild-type CXCL8 are Ala15, Arg26, and Cys50, [Fig. 4(A,C)]. Ala15 is located in the proximity of the binding site as shown in Figure 4(D) and Cys50 is directly involved in binding [Fig. 4(D) and Supporting Information Fig. S3A]. These elevated H(S/M)QC exchange induced shifts may further suggest that flexibility could play an important functional role in the binding interface of CXCL8. ^{15}N-R2 Carr-Purcell-Meiboom-Gill (CPMG) relaxation dispersion measurements were also collected to identify motions within the millisecond timescale.[35] However, we did not detect any measurable ^{15}N-R2-CPMG relaxation dispersion [Fig. 4(B)], suggesting that slow dynamics within wild-type CXCL8 are primarily confined to the μs timescale.

CXCL8M self-associates at high concentrations

Although the engineered CXCL8M mutant form has previously been described as a strictly monomeric species,[8] based on our NMR data we propose that this construct is able to dimerize with much weaker association constant than the wild-type. Although, it is possible that CXCL8M forms a higher order structure (i.e., oligomer) our NMR relaxation data supports the formation of a dimer along with previous studies conducted using different CXCL8 dimerization impaired constructs.[36] Specifically, as opposed to wild-type CXCL8, we observed detectable exchange in the ms regime for 14 out of 72 residues within CXCL8M as shown by ^{15}N-R2-CPMG dispersions that was concentration dependent [Fig. 5(A) dark green versus blue lines]. Both this concentration dependence and the fact that the regions undergoing exchange primarily localized to the dimerization interface suggest that CXCL8M is capable of dimerizing [Fig. 5(B)]. Moreover, all residues within CXCL8M exhibited similar dispersion profiles at the same concentration, which points to a global cooperative process (i.e., oligomerization). Utilizing dispersion data from two static magnetic fields [600 MHz and 900 MHz in Fig. 5(C), solid vs. dashed lines] allowed for the determination of the exchange rate between dimer/monomer (130 ± 30 s^{-1}) as well as the population of the dimer (7% dimer) at the 1 mM concentration used for the CXCL8M. Residues exhibiting exchange include the first β-strand, residues within the α-helix most proximal to the C-terminus and residues adjacent to the α-helix but positioned at the end of second and third β-strands [Fig. 5(B)]. Thus, in agreement with the previous biological study that provided evidence for monomeric mutants to partially dimerize,[36] our biophysical studies here provide further support for such an interaction. Caution should be taken in interpreting the R2 relaxation rates for CXCL8M, since several residues have contributions from exchange to the dimer. Nonetheless, despite the mutations to the dimer interface that induce dimer dissociation, our results suggest that CXCL8M does dimerize weakly within the millimolar concentrations utilized for NMR, highly suggestive of a self-association affinity within this millimolar range.

Chemical shift-based calculations identify fast time scale dynamics

Chemical shifts have long been used to predict protein structural propensities.[37] More recently, it has been shown that it is possible to increase the amount of information that can be extracted from them by introducing methods to translate chemical shifts directly into protein structures[38,39] and protein structural fluctuations.[40] This latter approach provides a complementary route to the use of relaxation data to study protein dynamics. In this context, the use of unrestrained molecular dynamics simulations provides a powerful tool for interpreting relaxation data, as shown recently by Skrynnikov *et al.*[40] However, since this type of analysis requires millisecond long trajectories, we analyzed here the equilibrium fluctuations of CXCL8 and CXCL8M using molecular dynamics simulations with chemical shift restraints.

The differential binding between CXCL8 and CXCL8M suggests that there may be an underlying difference in the structure and/or dynamics between the two forms. Thus, we analyzed our assigned carbon chemical shifts using the δ2D method,[41,42] which translates the chemical shifts into the secondary structure populations. The comparison of the results for free CXCL8 [Fig. 6(A)—left panel] and

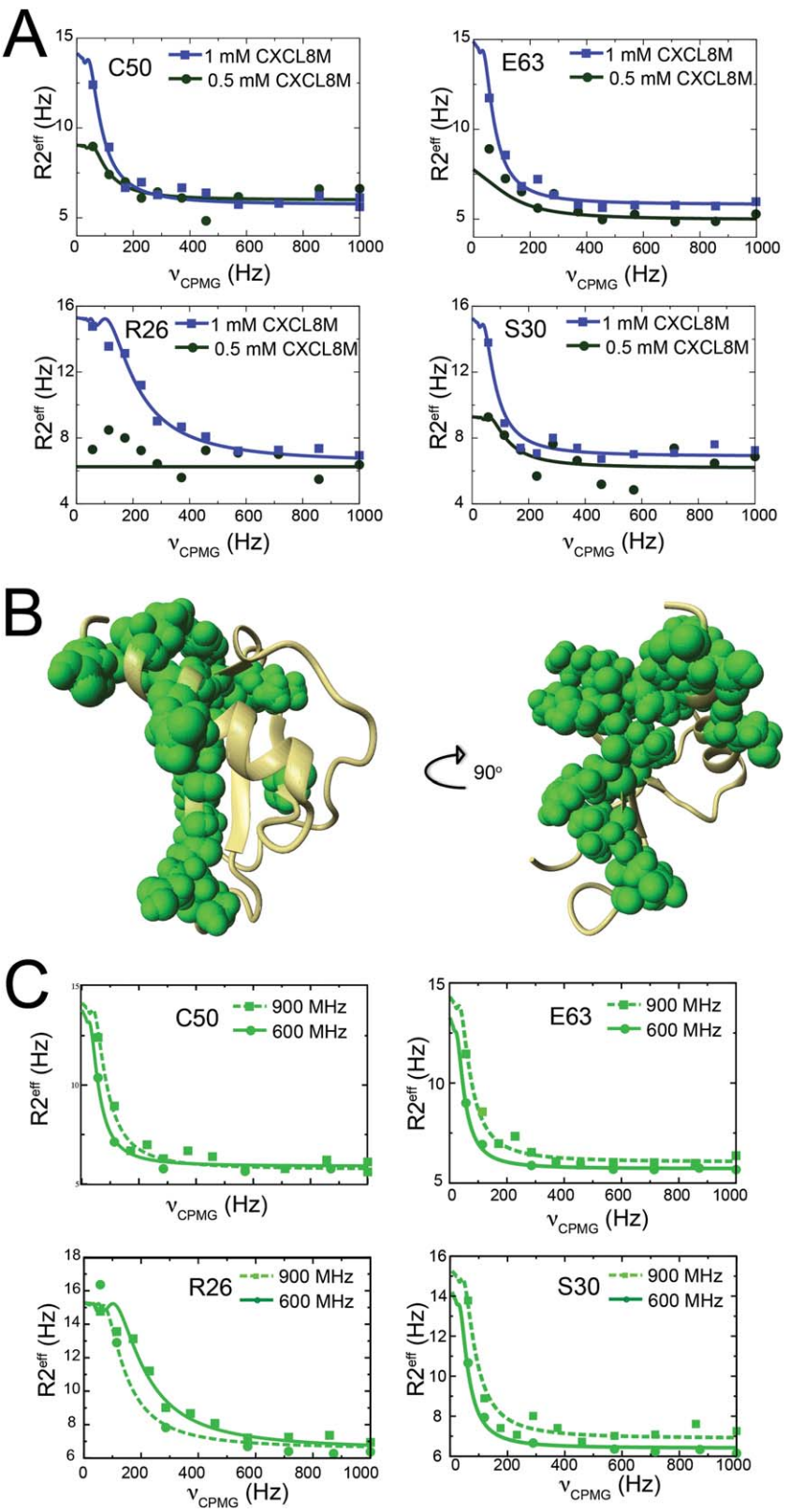

Figure 5. CXCL8M weakly dimerizes. (A) R2-CPMG dispersion data for representative residues (C50, E63, R26, and S30) at two different protein concentrations (1 m*M*—blue, 0.5 m*M*—green) (B) The residues exhibiting elevated R2-CPMG dispersion values are mapped onto the structure. (C) R2-CPMG dispersion data for representative residues (C50, E63, R26, and S30) at two different fields (900 MHz—dashed green, 600 MHz—solid green). PDB code 3IL8. All NMR experiments within this figure were collected in HEPES buffer at 25°C and at 600 MHz or 900 MHz.

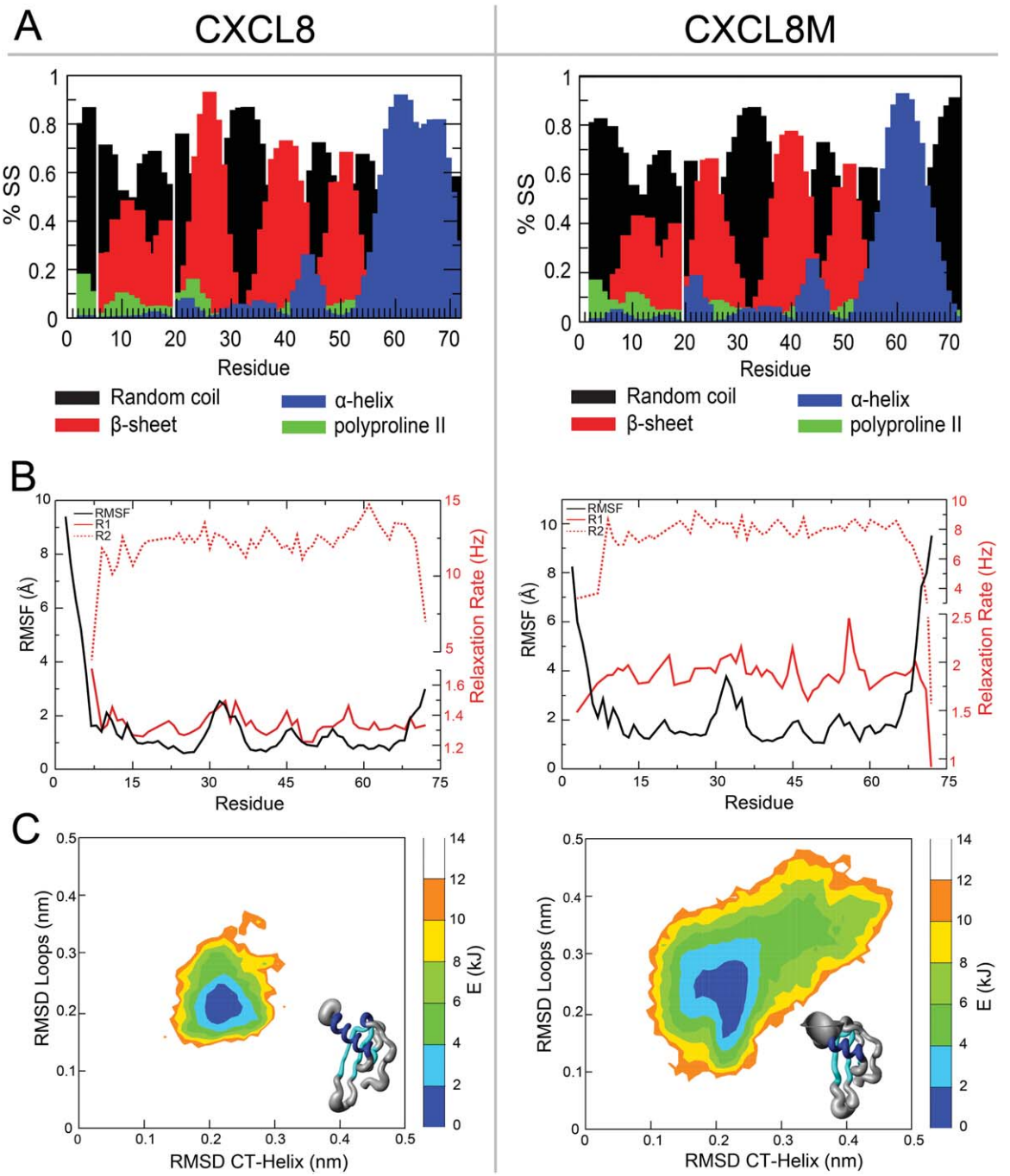

Figure 6. Chemical shift-based calculations correspond to fast time scale dynamics and reveal that the C-terminal helix of the CXCL8 monomer partially unfolds. (A) Secondary structure populations (SS%) calculated from the chemical shifts using the δ2D method (Berjanskii and Wishart)[37] for free CXCL8 (A—left panel) and CXCL8M (A—right panel); α-helix is shown in blue, β-sheet in red, polyproline II in green and random coil in black. (B) Local root mean square fluctuations (RMSF, solid black lines) are calculated for each amide from the ensemble of structures using chemical shift-based distance restraints and are plotted for free CXCL8 (B—left panel) and free CXCL8M (B—right panel) in phosphate buffer. NMR amide relaxation rates R2 (dashed red lines) and R1 (solid red lines) collected for the free CXCL8 (B—left panel) free CXCL8M (B—right panel) in phosphate buffer. (C) Free energy landscapes as a function of the RMSD of the C-terminal α-helix (CT-Helix, *x*-axis) and the RMSD of the two loops corresponding to residues 28 to 31 and 50 to 53 (RMSD-Loops, *y*-axis) for free CXCL8 (C—left panel) and free CXCL8M (C—right panel). The RMSDs were calculated for each conformation in the ensembles generated here against structures available in PDB for the α-helix and two loops, respectively. The energy is in kJ/mol. (C—structure inserts) From the chemical shift-based calculations, sausage models were calculated based on the local RMSD for both free CXCL8 (C—structure inserts, left panel) and free CXCL8M (C—structure inserts, right panel). For clarity purposes residues 1 to 7 are omitted from the MD structures. All data within this figure were collected in phosphate buffer at 25°C at 600 MHz.

free CXCL8M [Fig. 6(A)—right panel] indicate that the C-terminal α-helix is less well formed in the mutant, and that there is an overall increase in fluctuations in the regions corresponding to the β-sheet. Interestingly, the N-terminal region of CXCL8M appears to be slightly less flexible as compared to CXCL8, while there is increased flexibility in CXCL8M in two loops comprising residues 28 to 31 and 50 to 53 [Fig. 6(B)]. These data, for both CXCL8 and CXCL8M, are consistent with the relaxation data that identified similar flexible regions [Fig. 3(A)]. To gain further insight into these structural differences, we utilized our chemical shift data for both CXCL8 and CXCL8M in molecular dynamics simulations employing chemical shifts as replica-averaged restraints.[40] Since these chemical shifts were initially assigned in phosphate buffer, we also collected relaxation data in this same buffer [Fig. 6(B)], which were similar to those relaxation rates collected in HEPES buffer presented above [Fig. 3(A)]. Interestingly, local RMSFs calculated for both the dimeric and monomeric forms are largely mirrored by the R1 relaxation rate [Fig. 6(B), solid black vs. solid red lines], suggesting that the calculated ensembles here are largely descriptive of the fast time scale dynamics. A possible reason that the R2 relaxation rates may not match as well is that they may have contributions from slower motions that are not necessarily captured within the chemical shift-based calculations. As for the fundamental difference between the dimer and monomer, the increased disorder within the C-terminal region and two loops comprising residues 28 to 31 and 50 to 53 can readily be visualized with a partial unfolding of the C-terminal α-helix in CXCL8M relative to the wild-type CXCL8 dimer [Fig. 6(C)]. These results are illustrated particularly clearly by comparing the free energy landscapes of CXCL8 and CXCL8M as a function of the RMSD of the C-terminal α-helix and the RMSD of the two loop regions [Fig. 6(C)].

Discussion and Conclusions

In this study we have investigated the binding of CXCL8 to a peptide corresponding to the N-terminal region of human CXCR1. Our results support previous NMR solution findings in which the interaction between CXCL8 and hCXCR1 appears to be weak with micromolar dissociation constants.[19] However, our report is the first to utilize NMR relaxation data to show that, upon engagment of the human receptor peptide, the dimer does not dissociate as previously proposed.[7,15] These results suggest that at physiological concentrations, where both the CXCL8 dimer and monomer are likely to exist, both forms may initiate the interaction with the receptor. Biological data indicate that in some cases the CXCL8 dimer is more active than the monomer, but there are other cases in which the reverse is true.[36] For example, several biological studies demonstrate that dimerization deffective CXCL8 mutants (i.e., monomeric CXCL8 at experimental concentrations) are less active in colony formation in myeloid progenitor cells and inhibition of TNF-α stimulated peroxide induction in neutrophils.[8,43,44] Contrary to this, at low concentrations a trapped CXCL8 monomer was shown to be more active than the wild-type CXCL8 dimer in neutrophil migration.[18] Our biophysical studies indicate that a mutational variant of CXCL8 designed to remain monomeric (CXCL8M) binds only slightly more tightly to hCXCR1pep (Fig. 2). However, a recent elegant study in lipid bilayers has shown that CXCL8 binds much tighter to the N-terminal regions of CXCR1 in these conditions than in the absence of lipids.[17] This result may warrant further comparitive studies between CXCL8 and CXCL8 monomeric mutants to discern if this difference in affinity holds in the context of lipids.

One of the most remarkable findings in the field of protein dynamics has been that many enzymes are inherently flexible within the regions required for binding. For example, enzymes like cyclophilin-A,[30,34] dyhydrofolate reductase,[45] and RNAse A[46] exhibit conformational dynamics within their catalytic sites that are critical for catalytic turnover. However, such inherently flexible regions are likely ubquitiously present within non-catalytic proteins as well, such as cytokines that target multiple receptors which may also be flexible in order to allow for differential engagement. A case in point is interleukin-3 (IL-3), which has previously been shown to exhibit dynamics on multiple timescales which have been suggested to allow for binding promiscuity to multiple α-receptor subunits.[47] Our data presented here provides preliminary evidence for a similar trend with CXCL8. Specifically, we show some evidence that there may be inherent mobility localized to the hCXCR1pep binding region [Fig. 4(D)]. These motions include ps-ns dynamics identified through R1/R2 relaxation rates [Figs. 3(A) and 6(B)]. Additionally, the presence of elevated H(S/M)QC exchange induced shifts with no observable R2-CPMG dispersion in the CXCL8 dimer indicates that slower motions are likely confined to the μs timescale [Fig. 4(A,B)]. These results may support the view that proteins, such as enzymes and ligands, have evolutionarily evolved to have a flexibility compatible with their function.[30] This view also implies that proteins can undergo conformational selection in order to target their binding partners.[32]

Chemical shift-based calculations have recently become a powerful method to probe structure and dynamics of proteins and here we utilized such methods to compare the structural integrity of wild-type CXCL8 dimers with that of the mutated CXCL8 monomers. Initial clues to the structural differences between the CXCL8 dimer and monomer

were observed in both the relaxation data (Figs. 3 and 6) and RMSF [Fig. 6(B)]. Chemical shift-based calculations revealed an unfolding of the C-terminal region of the CXCL8 monomer [Fig. 6(B,C)], which is involved in stabilization of the CXCL8 dimer. Such flexibility in the CXCL8M may also explain the slightly tighter binding affinity relative to the CXCL8 dimer. This result likely leads to more interactions between the C-terminal α-helix of the CXCL8 monomer with hCXCR1pep that is supported by increased chemical shift perturbations (Supporting Information Fig. S3). Interestingly, the local RMSFs for both the CXCL8 dimer and monomer were highly predictive of the R1 relaxation rates, suggesting a link between these ensembles and fast dynamics [Fig. 6(B)]. Finally, we provided evidence to support supposition that the mutated form of CXCL8 (i.e., CXCL8M) dimerizes at high concentrations. Consistent with previous findings,[8] this CXCL8 mutant form is predominantly a monomeric species as indicated by size exclusion chromatography (data not shown) and also via correlation time measurements [Fig. 3(C)]. However, ^{15}N-R2-CPMG relaxation dispersion data provided an additional method to probe for self-association and revealed a concentration-dependent self-association through the dimer interface (Fig. 5). Furthermore, our restrained molecular dynamics simulation data supports the ^{15}N-R2-CPMG relaxation dispersion results by showing that the most energetically favorable conformations sampled by CXCL8M are highly similar to those sampled by wild-type CXCL8 [Fig. 6(C)]. Although, overall CXCL8M samples a much broader free energy landscape than its wild-type counterpart. This similarity in location of the lowest part of the free energy landscape provides further evidence that CXCL8M is capable of dimerizing.

Our data is in accordance with previously reported findings, which provided evidence that CXCL8 dimerization incapable constructs are still capable of forming dimers.[36] The possibility of an oligomer formation should also be noted, Schnitzel *et al.*,[48] presented evidence that CXCL8 can form oligomers, however, this was only observed in cell based studies and likely includes other cellular interactions. Thus far, both crystallographic and NMR-studies have established monomeric and dimeric structures of different CXCL8 constructs with no additional evidence for oligomer formation.[6,22,49] The possibility of dimer formation for the CXCL8 monomeric construct is an important finding since several different CXCL8 mutants are commonly used for biological and biophysical studies. Our data shows that caution must be taken when evaluating the results of such studies, as dimerization still persists at higher concentrations. Although such a dimerization may not initially appear to be a problem at the lower concentrations used for assaying CXCL8 biological activities, elevated local concentrations may give rise to dimer formation and, thus, should be recognized as a potential complicating factor.

In conclusion, we have shown through NMR solution studies that CXCL8 dimers do not dissociate upon binding to the N-terminal region of human CXCR1. Moreover, we have described how the differences in the previously reported binding affinities of CXCL8 to CXCR1 arise at least in part from the electrostatic nature of this interaction, which was studied here by comparative measurements in both phosphate and HEPES buffers. These results have important implications in the design of therapeutics that may specifically target CXCL8, as they suggest that both the dimeric and monomeric forms of CXCL8 will likely have to be targeted simultaneously in order to block the pro-inflammatory activities of this chemokine.

Materials and Methods

Protein expression, purification, and sample preparation

DNA encoding the 72 amino acid wild-type human CXCL8 was commercially purchased (Genewiz, South Planfield, NJ), PCR amplified, and subsequently ligated into the pET15b plasmid between NdeI and BamH1 sites for expression in E. Coli strain BL21 (DE3). The pET15b plasmid expression vector (Novagen Inc., Madison, WI) containing a 6xHis tag and thrombin cleavage site was used for initial CXCL8 protein expressions to generate CXCL8$^{\text{Synthetic}}$, containing a postcleavage GSHM overhang. In addition, a Factor Xa cleavage site (IEGR) was engineered directly C-terminal to the thrombin cleavage site (LVPRGS) in order to obtain the wild-type (no overhang) fully active sequence of CXCL8 (starting with SAK). Two CXCL8 constructs were inserted into these vectors, which included wild-type human full length CXCL8 and a monomeric variant (CXCL8M) obtained by performing site directed mutagenesis to acquire L25Y and V27R double mutant.[8] CXCL8 protein (wild-type and monomeric) was grown in LB or M9 minimal media supplemented with ^{15}N-ammonium chloride and/or ^{13}C-glucose for generation of unlabeled, ^{15}N or ^{15}N/^{13}C labeled samples. Proteins were refolded from the insoluble fractions as previously described[30] and subsequently purified via a Ni-affinity column followed by cleavage of the 6xHis tag with thrombin or Factor Xa (NEB, Ipswich, MA) and then size exclusion chromatography. All purifications were conducted on an AKTA FPLC system (GE Healthcare). Final samples for NMR contained 0.2 to 1.0 m*M* protein in NMR buffers: phosphate (50 m*M* Na_3PO_4, 150 m*M* NaCl pH 6.5) or HEPES (50 m*M* HEPES, 50 m*M* NaCl, pH 7.0) supplemented with 5% D_2O.

Peptide expression and purification

For peptide purification, a previously described protocol was applied with slight modifications.[50] Briefly,

standard PCR amplification methods were used to generate a construct containing amino acids corresponding to residues 9 to 29 of hCXCR1 (MWDFDDLNFTGMPPADEDYSP). The hCXCR1 peptide construct was cloned into a pet15b vector containing the small GB1 protein derived from streptococcal protein G, a 6xHis tag followed by a thrombin cleavage site, and then residues 9 to 29 of hCXCR1. This fusion protein was expressed in BL21 (DE3) cells in LB or isotope enriched media (see above for media composition). After Ni-affinity, thrombin was used to release the peptide and followed by HPLC purification. Peptide fractions from HPLC purification were lyophilized, resuspended in NMR buffer (phosphate or HEPES), and the pH adjusted appropriately. The identity of peptide was also confirmed via mass spectrometry using a MALDI-TOF instrument.

NMR spectroscopy and analysis

All NMR spectra were collected at 25°C on a Varian 600 MHz or 900 MHz spectrometer with samples supplemented with 5% D_2O. Samples utilized for assignment purposes contained 0.5 to 1 m*M* protein, while all samples used for titrations contained 0.2 to 0.5 m*M* protein with the indicated final concentration of the titrant. All spectra were processed using NMRPipe software[51] and analyzed using CCPNmr software.[52] Unless otherwise noted, all pulse sequences were obtained from standard Varian Biopack libraries. Standard multidimensional NMR experiments HNCACB, CBCA(CO)NH and HNCA were collected for each construct used, and both a 3D-^{15}N-NOESY and a 3D-^{15}N-TOCSY (total correlated spectroscopy) were used to confirm each spin system.

For relaxation experiments, standard R1 and R2 relaxation experiments were applied with recycle delays of 2.5 s at either 900 or 600 MHz. Relaxation delays for R1 experiments were 0.01, 0.1, 0.3, 0.5, 0.7, 0.9, and 1.1 s, and relaxation delays for R2 experiments were 0.01, 0.03, 0.05, 0.07, 0.11, and 0.13 s. While compensating pulses before the recycle delay were utilized for R2 measurements to account for potential sample heating, all relaxation experiments were arrayed within a single experiment to also account for any potential field inhomogeneities. Correlation times for each amide and free or bound protein were calculated using R2/R1 relaxation rate ratios as described in Larsson *et al*.[24] In-house scripts that combined both NMRPipe and Xmgrace software were used to fit and visualize, respectively, all relaxation rates using peak heights. The previously published correlation times (Supporting Information Table S1) were plotted versus molecular weight (MW) and the experimental MWs were estimated by fitting the experimental τ_c values into a least-squares linear regression equation ($\tau_c = 0.59 \times$ MW). ^{15}N-R2-CPMG pulse sequences were applied for relaxation dispersion experiments with the delay time of 0.05 s for CXCL8 and 0.07 for CXCL8M and H(S/M)QC pulse sequences were applied to measure exchange-induced shifts on a Varian 600 MHz spectrometer collected at 25°C.[33,53] Relaxation compensated pulse sequences for all ^{15}N-R2-CPMG experiments were also employed.

Molecular dynamics simulations

Replica-averaged restrained molecular dynamics simulations[41,42,54,55] were performed using GROMACS[56] coupled with PLUMED[57] and Almost.[58] The simulations were carried out using the Amber99SB*-ILDN force field[59] and the TIP3P water model. A time step of 2 fs was used together with LINCS constraints.[60] The van der Waals and electrostatic interactions were cut-off at 0.9 nm, and long-range electrostatic effects were treated with the particle mesh Ewald method.[61] All the simulations were done in the canonical ensemble by keeping the volume fixed and by thermosetting the system with the Bussi thermostat.[62] The starting conformations for both the monomer and the dimer were taken from an X-ray structure[49] (PDB code 1IL8). In the case of the monomer the L25Y and V27R mutations were modeled with PyMol.[63] The structures were protonated and solvated with 7000 water molecules in a dodecahedron box of 244 nm^3 of volume. The energy of the system was first minimized and then the temperature was increased to 300 K in two separate steps, in the first one a 50 ps long simulation was performed by keeping fixed the heavy atoms of the protein, and successively a second 200 ps long simulation was performed without restraints. The density of the system has been relaxed by a 200 ps long run using the Berendsen barostat. We carried out molecular dynamics simulations with replica-averaged chemical shift restraints, using four replicas.[54] The starting structures for the four replicas were selected as the final structure from four 1ns simulations. Each replica was evolved through a series of annealing cycles between 300 K and 400 K, each cycle being composed of 100 ps at 300 K, 100 ps of linear increase in the temperature up to 400 K, 100 ps of constant temperature molecular dynamics simulations at 400 K and 300 ps of linear decrease in the temperature to 300 K. Only structures from the 300 K portions of the simulations were taken into account for analysis. Each replica was evolved for 150 ns. The resulting ensemble is composed by all the structures sampled at 300 K by all the replicas after discarding the first 10 ns.

Statistical analysis

GraphPad Prism software (GraphPad Prism Software Inc., la Jolla, CA) was used to determine the binding isotherms. Only residues exhibiting fast exchange were included with amides that exhibit

chemical shift changes above the digital resolution of the indirect dimension (~0.6 ppm). These residues were simultaneously fit using nonlinear least square fit to the equation $\Delta\delta_{obs} = \Delta\delta_{sat} \times ([Ligand]_{tot} + [Protein]_{tot} + K_d - (([Ligand]_{tot} + [Protein]_{tot} + Kd)^2 - 4 \times [Ligand]_{tot} \times [Protein]^5)/(2 \times [Protein]_{tot})$, where $\Delta\delta_{obs}$ (normalized chemical change as defined by $\sqrt{(5\Delta v_{1H})^2 + (\Delta v_{15N})^2}$) is the observed $\Delta\delta$ at the given Ligand concentration, $\Delta\delta_{sat}$ is the $\Delta\delta$ at saturation. Protein is the specific CXCL8 construct used at a constant total concentration ($[Protein]_{tot}$) for each titration experiment and ($[Ligand]_{tot}$ is CXCR1pep or $CXCL8^{synthetic}$ (see Supporting Information Fig. S2) at a specific total concentration for the respective titration point.

Acknowledgments

NMR experiments were collected at several facilities described herein. Part of the data was acquired at the High Magnetic Field Laboratory (NHMFL), which is supported by cooperative agreement between the National Science Foundation and the State of Florida. A portion of NMR data collection was performed at the Environmental Molecular Sciences Laboratory, a national scientific user facility sponsored by the Department of Energy's Office of Biological and Environmental Research and located at Pacific Northwest National Laboratory. The Rocky Mountain 900 Facility was also used for NMR data collection.

References

1. Waugh DJJ, Wilson C (2008) The interleukin-8 pathway in cancer. Clin Cancer Res 14:6735–6741.
2. Mackay CR (2001) Chemokines: immunology's high impact factors. Nat Immunol 2:95–101.
3. Allen SJ, Crown SE, Handel TM (2007) Chemokine: receptor structure, interactions, and antagonism. Annu Rev Immunol 25:787–820.
4. Fernandez EJ, Lolis E (2002) Structure, function, and inhibition of chemokines. Annu Rev Pharmacol Toxicol 42:469–499.
5. Fernando H, Nagle GT, Rajarathnam K (2007) Thermodynamic characterization of interleukin-8 monomer binding to CXCR1 receptor N-terminal domain. FEBS J 274:241–251.
6. Rajarathnam K, Clarklewis I, Sykes BD (1995) H-1-NMR solution structure of an active monomeric interleukin-8. Biochemistry 34:12983–12990.
7. Ravindran A, Joseph PR, Rajarathnam K (2009) Structural basis for differential binding of the interleukin-8 monomer and dimer to the CXCR1 N-domain: role of coupled interactions and dynamics. Biochemistry 48: 8795–8805.
8. Daly TJ, LaRosa GJ, Dolich S, Maione TE, Cooper S, Broxmeyer HE (1995) High activity suppression of myeloid progenitor proliferation by chimeric mutants of interleukin 8 and platelet factor 4. J Biol Chem 270: 23282–23292.
9. Skelton NJ, Quan C, Reilly D, Lowman H (1999) Structure of a CXC chemokine-receptor fragment in complex with interleukin-8. Structure 7:157–168.
10. Nasser MW, Raghuwanshi SK, Grant DJ, Jala VR, Rajarathnam K, Richardson RM (2009) differential activation and regulation of CXCR1 and CXCR2 by CXCL8 monomer and dimer. J Immunol 183:3425–3432.
11. Burrows SD, Doyle ML, Murphy KP, Franklin SG, White JR, Brooks I, McNulty DE, Scott MO, Knutson JR, Porter D, Young PR, Hensley P (1994) Determination of the monomer-dimer equilibrium of interleukin-8 reveals it is a monomer at physiological concentrations. Biochemistry 33:12741–12745.
12. Clark-Lewis I, Schumacher C, Baggiolini M, Moser B (1991) Structure-activity relationships of interleukin-8 determined using chemically synthesized analogs. Critical role of NH2-terminal residues and evidence for uncoupling of neutrophil chemotaxis, exocytosis, and receptor binding activities. J Biol Chem 266:23128–23134.
13. Ginestier C, Liu SL, Diebel ME, Korkaya H, Luo M, Brown M, Wicinski J, Cabaud O, Charafe-Jauffret E, Birnbaum D, Guan JL, Dontu G, Wicha MS (2010) CXCR1 blockade selectively targets human breast cancer stem cells in vitro and in xenografts. J Clin Invest 120:485–497.
14. Holmes WE, Lee J, Kuang WJ, Rice GC, Wood WI (1991) Structure and functional expression of a human interleukin-8 receptor. Science 253:1278–1280.
15. Fernando H, Chin C, Rosgen J, Rajarathnam K (2004) Dimer dissociation is essential for interleukin-8 (IL-8) binding to CXCR1 receptor. J Biol Chem 279:36175–36178.
16. Rajarathnam K, Prado GN, Fernando H, Clark-Lewis I, Navarro J (2006) Probing receptor binding activity of interleukin-8 dimer using a disulfide trap. Biochemistry 45:7882–7888.
17. Park SH, Casagrande F, Cho L, Albrecht L, Opella SJ (2011) Interactions of interleukin-8 with the human chemokine receptor CXCR1 in phospholipid bilayers by NMR spectroscopy. J Mol Biol 414:194–203.
18. Das ST, Rajagopalan L, Guerrero-Plata A, Sai J, Richmond A, Garofalo RP, Rajarathnam K (2010) Monomeric and dimeric CXCL8 are both essential for in vivo neutrophil recruitment. PLoS One 5:e11754.
19. Clubb RT, Omichinski JG, Clore GM, Gronenborn AM (1994) Mapping the binding surface of interleukin-8 complexed with an N-terminal fragment of the type-1 human interleukin-8 receptor. FEBS Lett 338:93–97.
20. Rajagopalan L, Rajarathnam K (2004) Ligand selectivity and affinity of chemokine receptor CXCR1. Role of N-terminal domain. J Biol Chem 279:30000–30008.
21. Leong SR, Kabakoff RC, Hebert CA (1994) Complete mutagenesis of the extracellular domain of interleukin-8 (IL-8) type A receptor identifies charged residues mediating IL-8 binding and signal transduction. J Biol Chem 269:19343–19348.
22. Baldwin ET, Weber IT, St Charles R, Xuan JC, Appella E, Yamada M, Matsushima K, Edwards BF, Clore GM, Gronenborn AM, Wlodawer A (1991) Crystal structure of interleukin 8: symbiosis of NMR and crystallography. Proceedings of the National Academy of Sciences of the United States of America 88:502–506.
23. Gerety SJ, Karpus WJ, Cubbon AR, Goswami RG, Rundell MK, Peterson JD, Miller SD (1994) Class II-restricted T cell responses in Theiler's murine encephalomyelitis virus-induced demyelinating disease. V. Mapping of a dominant immunopathologic VP2 T cell epitope in susceptible SJL/J mice. J Immunol 152:908–918.
24. Larsson G, Martinez G, Schleucher J, Wijmenga SS (2003) Detection of nano-second internal motion and

determination of overall tumbling times independent of the time scale of internal motion in proteins from NMR relaxation data. J Biomol NMR 27:291–312.
25. Lee D, Hilty C, Wider G, Wuthrich K (2006) Effective rotational correlation times of proteins from NMR relaxation interference. J Magn Reson 178:72–76.
26. Rossi P, Swapna GV, Huang YJ, Aramini JM, Anklin C, Conover K, Hamilton K, Xiao R, Acton TB, Ertekin A, Everett JK, Montelione GT (2010) A microscale protein NMR sample screening pipeline. J Biomol NMR 46:11–22.
27. Taylor GM, Ma L, Vogt VM, Post CB (2010) NMR relaxation studies of an RNA-binding segment of the rous sarcoma virus gag polyprotein in free and bound states: a model for autoinhibition of assembly. Biochemistry 49:4006–4017.
28. Kay LE, Torchia DA, Bax A (1989) Backbone dynamics of proteins as studied by 15N inverse detected heteronuclear NMR spectroscopy: application to staphylococcal nuclease. Biochemistry 28:8972–8979.
29. Kojima C, Ono A, Kainosho M, James TL (1999) Quantitative measurement of transverse and longitudinal cross-correlation between 13C-1H dipolar interaction and 13C chemical shift anisotropy: application to a 13C-labeled DNA duplex. J Magn Reson 136:169–175.
30. Eisenmesser EZ, Millet O, Labeikovsky W, Korzhnev DM, Wolf-Watz M, Bosco DA, Skalicky JJ, Kay LE, Kern D (2005) Intrinsic dynamics of an enzyme underlies catalysis. Nature 438:117–121.
31. Henzler-Wildman K, Kern D (2007) Dynamic personalities of proteins. Nature 450:964–972.
32. Boehr DD, Dyson HJ, Wright PE (2006) An NMR perspective on enzyme dynamics. Chem Rev 106:3055–3079.
33. Skrynnikov NR, Dahlquist FW, Kay LE (2002) Reconstructing NMR spectra of "invisible" excited protein states using HSQC and HMQC experiments. J Am Chem Soc 124:12352–12360.
34. Schlegel J, Armstrong GS, Redzic JS, Zhang F, Eisenmesser EZ (2009) Characterizing and controlling the inherent dynamics of cyclophilin-A. Protein Sci 18:811–824.
35. Mulder FA, Skrynnikov NR, Hon B, Dahlquist FW, Kay LE (2001) Measurement of slow (micros-ms) time scale dynamics in protein side chains by (15)N relaxation dispersion NMR spectroscopy: application to Asn and Gln residues in a cavity mutant of T4 lysozyme. J Am Chem Soc 123:967–975.
36. Lowman HB, Fairbrother WJ, Slagle PH, Kabakoff R, Liu J, Shire S, Hebert CA (1997) Monomeric variants of IL-8: effects of side chain substitutions and solution conditions upon dimer formation. Protein Sci 6:598–608.
37. Berjanskii MV, Wishart DS (2005) A simple method to predict protein flexibility using secondary chemical shifts. J Am Chem Soc 127:14970–14971.
38. Cavalli A, Salvatella X, Dobson CM, Vendruscolo M (2007) Protein structure determination from NMR chemical shifts. Proc Natl Acad Sci USA 104:9615–9620.
39. Shen Y, Lange O, Delaglio F, Rossi P, Aramini JM, Liu GH, Eletsky A, Wu YB, Singarapu KK, Lemak A, Ignatchenko A, Arrowsmith CH, Szyperski T, Montelione GT, Baker D, Bax A (2008) Consistent blind protein structure generation from NMR chemical shift data. Proc Natl Acad Sci USA 105:4685–4690.
40. Xue Y, Ward JM, Yuwen T, Podkorytov IS, Skrynnikov NR (2012) Microsecond time-scale conformational exchange in proteins: using long molecular dynamics trajectory to simulate NMR relaxation dispersion data. J Am Chem Soc 134:2555–2562.
41. Camilloni C, Robustelli P, De Simone A, Cavalli A, Vendruscolo M (2012) Characterization of the conformational equilibrium between the two major substates of RNase A using NMR chemical shifts. J Am Chem Soc 134:3968–3971.
42. Camilloni C, De Simone A, Vranken WF, Vendruscolo M (2012) Determination of secondary structure populations in disordered states of proteins using nuclear magnetic resonance chemical shifts. Biochemistry 51:2224–2231.
43. Williams MA, Cave CM, Quaid G, Robinson C, Daly TJ, Witt D, Lentsch AB, Solomkin JS (2005) Interleukin 8 dimerization as a mechanism for regulation of neutrophil adherence-dependent oxidant production. Shock 23:371–376.
44. Horcher M, Rot A, Aschauer H, Besemer J (1998) IL-8 derivatives with a reduced potential to form homodimers are fully active in vitro and in vivo. Cytokine 10:1–12.
45. Osborne MJ, Wright PE (2001) Anisotropic rotational diffusion in model-free analysis for a ternary DHFR complex. J Biomol NMR 19:209–230.
46. Cole R, Loria JP (2002) Evidence for flexibility in the function of ribonuclease A. Biochemistry 41:6072–6081.
47. Yao S, Young IG, Norton RS, Murphy JM (2011) Murine interleukin-3: structure, dynamics, and conformational heterogeneity in solution. Biochemistry 50:2464–2477.
48. Schnitzel W, Monschein U, Besemer J (1994) Monomer-dimer equilibria of interleukin-8 and neutrophil-activating peptide 2. Evidence for IL-8 binding as a dimer and oligomer to IL-8 receptor B. J Leuk Biol 55:763–770.
49. Clore GM, Appella E, Yamada M, Matsushima K, Gronenborn AM (1990) Three-dimensional structure of interleukin 8 in solution. Biochemistry 29:1689–1696.
50. Schlegel J, Redzic JS, Porter C, Yurchenko V, Bukrinsky M, Armstrong GS, Zhang FL, Isern NG, DeGregori J, Hodges R, Eisenmesser EZ (2009) Solution characterization of the extracellular region of CD147 and its interaction with its enzyme ligand cyclophilin-A. J Mol Biol 391:518–535.
51. Delaglio F, Grzesiek S, Vuister GW, Zhu G, Pfeifer J, Bax A (1995) NMRPipe: a multidimensional spectral processing system based on UNIX pipes. J Biomol NMR 6:277–293.
52. Vranken WF, Boucher W, Stevens TJ, Fogh RH, Pajon A, Llinas M, Ulrich EL, Markley JL, Ionides J, Laue ED (2005) The CCPN data model for NMR spectroscopy: development of a software pipeline. Proteins 59:687–696.
53. Loria JP, Rance M, Palmer AG 3rd (1999) A TROSY CPMG sequence for characterizing chemical exchange in large proteins. J Biomol NMR 15:151–155.
54. Camilloni C, Cavalli A, Vendruscolo M (2013) Assessment of the use of NMR chemical shifts as replica-averaged structural restraints in molecular dynamics simulations to characterize the dynamics of proteins. J Phys Chem B 117:1838–1843.
55. Cavalli A, Camilloni C, Vendruscolo M (2013) Molecular dynamics simulations with replica-averaged structural restraints generate structural ensembles according to the maximum entropy principle. J Chem Phys 138:094112.
56. Pronk S, Pall S, Schulz R, Larsson P, Bjelkmar P, Apostolov R, Shirts MR, Smith JC, Kasson PM, van der Spoel D, Hess B, Lindahl E (2013) GROMACS 4.5: a high-throughput and highly parallel open source molecular simulation toolkit. Bioinformatics 29:845–854.

57. Bonomi M, Branduardi D, Bussi G, Camilloni C, Provasi D, Raiteri P, Donadio D, Marinelli F, Pietrucci F, Broglia RA, Parrinello M (2009) PLUMED: a portable plugin for free-energy calculations with molecular dynamics. Comp Phys Commun 180:1961–1972.
58. Cavalli A, Vendruscolo M, Paci E (2005) Comparison of sequence-based and structure-based energy functions for the reversible folding of a peptide. Biophys J 88: 3158–3166.
59. Piana S, Lindorff-Larsen K, Shaw DE (2011) How robust are protein folding simulations with respect to force field parameterization? Biophys J 100:L47–49.
60. Hess B (2008) P-LINCS: A parallel linear constraint solver for molecular simulation. J Chem Theory Comput 4:116–122.
61. Essmann U, Perera L, Berkowitz ML, Darden T, Lee H, Pedersen LG (1995) A smooth particle mesh Ewald method. J Chem Phys 103:8577–8593.
62. Bussi G, Donadio D, Parrinello M (2007) Canonical sampling through velocity rescaling. J Chem Phys 126: 014101.
63. DeLano WL, Lam JW (2005) PyMOL: A communications tool for computational models. Abstr Pap Am Chem Soc 230: U1371–U1372.